Destruction of Potential Vorticity by Winds

LEIF N. THOMAS*

School of Oceanography, University of Washington, Seattle, Washington

(Manuscript received 10 January 2005, in final form 17 June 2005)

ABSTRACT

The destruction of potential vorticity (PV) at ocean fronts by wind stress–driven frictional forces is examined using PV flux formalism and numerical simulations. When a front is forced by "downfront" winds, that is, winds blowing in the direction of the frontal jet, a nonadvective frictional PV flux that is upward at the sea surface is induced. The flux extracts PV out of the ocean, leading to the formation of a boundary layer thicker than the Ekman layer, with nearly zero PV and nonzero stratification. The PV reduction is not only active in the Ekman layer but is transmitted through the boundary layer via secondary circulations that exchange low PV from the Ekman layer with high PV from the pycnocline. Extraction of PV from the pycnocline by the secondary circulations results in an upward advective PV flux at the base of the boundary layer that scales with the surface, nonadvective, frictional PV flux and that leads to the deepening of the layer. At fronts forced by both downfront winds and a destabilizing atmospheric buoyancy flux F^B_{atm}, the critical parameter that determines whether the wind or the buoyancy flux is the dominant cause for PV destruction is $(H/\delta_e)(F^B_{\text{wind}}/F^B_{\text{atm}})$, where H and δ_e are the mixed layer and Ekman layer depths, $F^B_{\text{wind}} = S^2\tau_o/(\rho_o f)$, S^2 is the magnitude of the lateral buoyancy gradient of the front, τ_o is the downfront component of the wind stress, ρ_o is a reference density, and f is the Coriolis parameter. When this parameter is greater than 1, PV destruction by winds dominates and may play an important role in the formation of mode water.

1. Introduction

In the upper-ocean mixed layer, the potential vorticity (PV) of surface waters is modified by frictional and diabatic processes until the fluid is subducted into the nearly inviscid, adiabatic interior. Once in the interior, the PV acts as a conservative, yet dynamically active, tracer whose large-scale spatial structure is of critical importance to the oceanic general circulation (Rhines 1986). A particular type of water mass with PV strongly modified by upper-ocean processes that affects gyre-scale flows is mode water (Hanawa and Talley 2000). Mode water is characterized by low PV and is associated with ocean fronts. The low PV signature of mode water suggests that PV destruction is critical to its creation. Mode water formation is commonly attributed to diabatic processes driven by wintertime buoyancy loss from the ocean surface associated with cold-air outbreaks (Worthington 1977). However, some mode water is formed in regions that lack cold-air outbreaks and significant buoyancy loss, as is the case in the Antarctic Circumpolar Current (Rintoul and England 2002). Although these regions are not forced by cold-air outbreaks, they are forced by winds, and it is possible that frictional forces associated with these winds could lead to PV destruction and contribute to mode water formation. To explore this possibility, in section 2 the PV equation is derived in its flux form to determine what type of wind forcing can reduce the PV, and in section 3 solutions of numerical simulations of a wind-forced frontal zone are described to elucidate how wind forcing destroys PV. The winds used to force the numerical simulations of section 3 have an orientation such that they drive Ekman flow that advects water from the dense side of the frontal zone over lighter waters, triggering convection. Since the numerical model used for the simulations is hydrostatic, this Ekman-driven convection must be parameterized. The parameterization of the Ekman-driven convection used involves a modification of the "K profile parameterization" (KPP) of Large et al. (1994) and is described in the appendix.

* Current affiliation: Woods Hole Oceanographic Institution, Woods Hole, Massachusetts.

Corresponding author address: Leif N. Thomas, Dept. of Physical Oceanography, WHOI, MS 21, Woods Hole, MA 02543.
E-mail: lthomas@whoi.edu

2. Potential vorticity dynamics

Under what atmospheric forcing conditions is the PV of the upper ocean reduced? To address this question and to understand the dynamics of the PV, it is instructive to derive a flux form for the PV equation similar to that by Haynes and McIntyre (1987) for atmospheric applications and adapted for the ocean by Marshall and Nurser (1992). In the next section, the PV flux formalism of Marshall and Nurser (1992) is summarized but modified for an incompressible, Boussinesq fluid on an f plane, approximations appropriate for upper-ocean, frontal dynamics.

In this paper a definition for the PV q is adopted similar to that used by Hoskins (1974):

$$q = f\omega_a \cdot \nabla b, \tag{1}$$

where $\omega_a = f\mathbf{k} + \nabla \times \mathbf{u}$ is the absolute vorticity (f is the Coriolis parameter, $\mathbf{k}$ is the vertical unit vector, and $\mathbf{u}$ is the velocity of the fluid); $b = -g\rho/\rho_o$ is the buoyancy (g is the gravitational acceleration, ρ is the density, and ρ_o is a reference density). The extra factor of f in (1) removes the ambiguity in the definition of PV reduction in either the Northern or Southern Hemisphere: when the value of the PV decreases—that is, when the fluid is drawn toward a state of gravitational, inertial, or symmetric instability where $q < 0$—the PV is reduced.

a. Flux form of the potential vorticity equation

Changes in the PV result from convergences/divergences of the PV flux; that is,

$$\frac{\partial q}{\partial t} = -\nabla \cdot \mathbf{J}, \tag{2}$$

where the PV flux

$$\mathbf{J} = q\mathbf{u} + f\nabla b \times \mathbf{F} - f\mathcal{D}\omega_a \tag{3}$$

has an advective constituent $q\mathbf{u}$ and nonadvective constituents that arise from diabatic processes $\mathcal{D}$:

$$\mathcal{D} \equiv \frac{\partial b}{\partial t} + \mathbf{u} \cdot \nabla \mathbf{b}, \tag{4}$$

and from frictional or nonconservative body forces $\mathbf{F}$:

$$\mathbf{F} \equiv \frac{\partial \mathbf{u}}{\partial t} + \mathbf{u} \cdot \nabla \mathbf{u} + f\hat{k} \times \mathbf{u} + \frac{1}{\rho_o}\nabla p, \tag{5}$$

where p is the pressure.

b. Conditions favorable for potential vorticity destruction at a front

To determine what conditions are favorable for PV destruction at a front, consider integrating (2) over a control volume that encircles the front. Application of Gauss's theorem to the integral reveals that reduction of the volume-averaged PV occurs when the net flux of PV through the surface of the control volume is outward. Consider the control volume $\mathcal{V}$ shown in Fig. 1 with an upper surface that coincides with the air–sea interface, side surfaces that are the isopycnals bounding the frontal zone, and a bottom surface that crosses isopycnals at a depth where the flow, frictional forces, diabatic processes, and hence PV fluxes are weak. For such a volume, only the PV flux out of the sea surface contributes to the change of volume-averaged PV since no PV is fluxed through the isopycnal surfaces of the control volume, in accordance with the "impermeability theorem" of Haynes and McIntyre (1987). Therefore, the PV in the control volume will be reduced if the PV flux at the sea surface is upward.

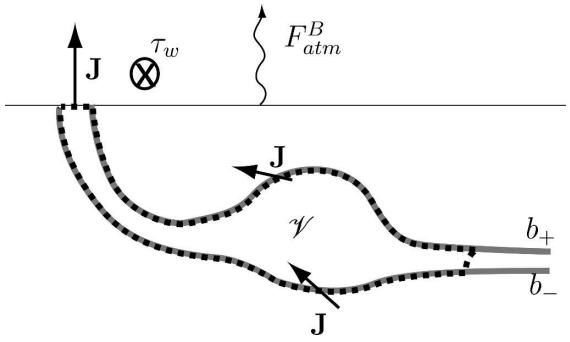

FIG. 1. A control volume $\mathcal{V}$ (dashed lines) with side surfaces coincident with isopycnals (gray contours) with buoyancy b_+ and b_- that bound the frontal zone. The "downfront" wind stress τ_w and flux of buoyancy from the ocean to the atmosphere F^B_{atm} will result in an upward PV flux $\mathbf{J}$ at the sea surface.

At the sea surface, in the limit of a rigid lid, the vertical velocity is zero or otherwise weak so that the vertical component of the PV flux is dominated by its nonadvective constituents. Under what atmospheric forcing condition is the nonadvective PV flux at the surface upward? For an inertially stable flow, where $f(f + \mathbf{k} \cdot \nabla \times \mathbf{u}) > 0$, diabatic processes will result in an upward PV flux

$$J^{\mathcal{D}}_z = -f(f + \mathbf{k} \cdot \nabla \times \mathbf{u})\mathcal{D} \tag{6}$$

when $\mathcal{D} < 0$. Diabatic processes will reduce the buoyancy, that is, $\mathcal{D} < 0$, when there is a net loss of buoyancy from the ocean to the atmosphere. This is not surprising, since buoyancy loss to the atmosphere triggers convective mixing that reduces the stratification, a process that has long been associated with the mechanism for the destruction of PV and the formation of mode waters at ocean fronts (Hanawa and Talley 2000). However, for fronts forced by winds, atmospheric buoyancy

loss is not the only contributor to PV destruction, the nonadvective flux associated with frictional forces can also play a critical role in reducing the PV, as will be demonstrated below.

The vertical component of the nonadvective PV flux associated with frictional forces

$$J_z^F = f\nabla_h b \times \mathbf{F} \tag{7}$$

is nonzero only if there is a horizontal buoyancy gradient $\nabla_h b$. Associating the horizontal buoyancy gradient with a vertically sheared geostrophic flow $\mathbf{u}_g$ via the thermal wind relation

$$\nabla_h b = f\frac{\partial \mathbf{u}_g}{\partial z} \times \mathbf{k}$$

reveals that the nonadvective PV flux associated with frictional forces

$$J_z^F = f^2 \frac{\partial \mathbf{u}_g}{\partial z} \cdot \mathbf{F} \tag{8}$$

is upward when the frictional force is in the direction of the geostrophic shear. For wind-forced flows, the frictional force is dominantly in the direction of the wind stress. Currents at upper-ocean fronts are usually surface intensified so that the surface current of the front is oriented with the geostrophic shear. Therefore, when the wind blows in the direction of the frontal jet, that is, is in a "downfront" orientation, the conditions are favorable for PV destruction by frictional forces (i.e., $J_z^F > 0$).

To understand how frictional forces can reduce the PV, consider the case of a geostrophic current with positive vertical shear forced by a purely downfront wind stress. In this configuration, the Ekman flow is directed along the horizontal buoyancy gradient and is sheared in the vertical causing denser water to be advected over lighter water, reducing the stratification. The sheared Ekman flow also tilts the planetary vorticity vector to the horizontal, which tends to generate PV-enhancing horizontal vorticity, that is, vorticity with $f\omega_a \cdot \nabla_h b > 0$. Tilting of planetary vorticity by the Ekman flow cannot compensate for the reduction of PV caused by the weakened stratification, however, because of the frictional torque supplied by the wind stress. In a steady Ekman layer, the frictional torque balances the tilting of planetary vorticity, pinning the horizontal vorticity to a steady value. Therefore, while the stratification is free to be weakened by the shearing motion of the Ekman flow, the horizontal vorticity remains fixed. This mechanism allows the PV in the Ekman layer to be destroyed.

c. Scaling for the potential vorticity fluxes

Upper-ocean fronts often experience both wind forcing and buoyancy loss. The question arises: what are the relative contributions to the PV reduction at a front by diabatic and frictional effects? To address this issue, consider the following scaling argument. Under conditions of atmospheric buoyancy loss, gravitational instability will result in a convective buoyancy flux that scales with the buoyancy loss to the atmosphere F^B_{atm}, and that decays nearly linearly with depth through the mixed layer of thickness H (Large et al. 1994). Therefore an appropriate scale for diabatic processes induced by buoyancy loss to the atmosphere is $\mathcal{D} \sim F^B_{\text{atm}}/H$, so that the scaling for (6) is

$$J_z^{\mathcal{D}} \sim f^2 \frac{F^B_{\text{atm}}}{H}. \tag{9}$$

A wind stress of strength τ_o will exert a frictional force of scale $F \sim \tau_o/\rho_o\delta_e$ over the turbulent Ekman layer of thickness $\delta_e = 0.4u^*/f$, where $u^* = \sqrt{\tau_o/\rho_o}$ is the friction velocity (Wimbush and Munk 1970). If the magnitude of the horizontal buoyancy gradient at the front is $S^2 = |\nabla_h b|$, then the appropriate scaling for (7) is

$$J_z^F \sim fS^2 \frac{\tau_o}{\rho_o \delta_e}. \tag{10}$$

The relative contributions of friction and diabatic effects to PV reduction can be assessed by taking the ratio of (10) and (9):

$$\frac{J_z^F}{J_z^{\mathcal{D}}} \sim \left(\frac{H}{\delta_e}\right)\left(\frac{F^B_{\text{wind}}}{F^B_{\text{atm}}}\right), \tag{11}$$

where $F^B_{\text{wind}} = S^2\tau_o/(\rho_o f)$, is a wind-driven buoyancy flux (WDBF) representing the flux of buoyancy exiting the fluid beneath the Ekman layer. The WDBF is required to balance the tendency of Ekman flow to reduce the buoyancy by lateral advection when the wind stress is downfront (Marshall and Nurser 1992; Straneo et al. 2002a; Thomas and Lee 2005).

Both the ratios of the WDBF to F^B_{atm}, and the mixed layer to Ekman layer depths have an effect on (11). It is conventionally assumed, and observations taken in conditions where $H \leq 100$ m indicate, that the Ekman and mixed layer depths are of the same order of magnitude (Chereskin and Roemmich 1991; Wijffels et al. 1994; Lee and Eriksen 1996). This suggests that the ratio H/δ_e does not greatly influence (11). Therefore, in the following discussion of the implications of (11) for mode water formation at fronts, the relative strengths

of the WDBF and F^B_{atm}, will be emphasized. Having stated this however, in regions of the ocean with deep mixed layers, the Ekman depth could be significantly smaller than H, in which case the discrepancy between H and δ_e should be considered in a discussion of PV destruction by atmospheric forcing.

On account of the strong lateral density gradients, at wind-forced fronts, the WDBF can be comparable to or larger than the atmospheric buoyancy loss, making the ratio (11) greater than or equal to 1. This even holds at subpolar fronts in the Northern Hemisphere forced by wintertime cold-air outbreaks that extract large amounts of heat from the ocean, yet also force the fronts strongly with downfront wind stress. For example, using hydrographic measurements combined with shipboard meteorological data taken at the subpolar front of the Japan/East Sea during a cold-air outbreak Thomas and Lee (2005) estimated the WDBF to be an order of magnitude larger than the atmospheric buoyancy flux, even with the heat loss of $\sim$500 W m^{-2} experienced at the front. The influence of wind-driven PV reduction at fronts may be even more pronounced in the Southern Ocean where fronts are forced by strong downfront winds and relatively weak air–sea fluxes of heat and freshwater (Rintoul and England 2002). In summary, these simple scaling arguments suggest that for fronts forced by downfront winds, PV reduction by wind stress can be at least as important as that due to heat loss and therefore should be accounted for in the formation of mode waters.

3. Numerical experiments

In the previous section, it was shown that forcing of fronts by downfront winds leads to a reduction of the volume-averaged PV. However, the utility of volume averages is limited because they do not shed light on the detailed structure of the PV and how it is destroyed. To investigate in detail how frictional forces by downfront winds destroy PV at a front, numerical experiments of a wind-forced frontal zone were performed, the solutions of which are described below.

a. Numerical model configuration

For the numerical experiments presented in this paper, the idealized frontal zone configuration of Thomas and Lee (2005) was used. The frontal zone consists of a laterally homogeneous, baroclinic, zonal flow $U = S^2/fz$ in a thermal wind balance with a buoyancy field B characterized by uniform lateral gradient $\partial B/\partial y = -S^2$ and a vertically varying stratification:

$$\frac{\partial B}{\partial z} = \begin{cases} N^2_{\text{ml}} & z > -H \\ N^2_{\text{ml}} - \dfrac{S^4}{f^2\delta}(z + H) & z < -H, \end{cases}$$

where $N^2_{\text{ml}} = 0.9S^4/f^2$, $H = 38$ m, and $\delta = 3.8$ m. In the surface layer, that is, $z > -H$, the PV is spatially uniform and small in magnitude. By choosing the value of the initial PV to be low in the surface layer, it has been assumed that the frontal zone is located in a region frequently exposed to cooling and/or downfront winds so that at sometime previous to the start of the experiment the low-PV surface layer was formed. The increase in stratification beneath $z = -H$ is meant to be a simple representation of a pycnocline, a region of high PV that can be eroded away by PV-reducing wind forcing. The frontal zone is forced by a spatially uniform downfront wind stress of strength τ_o turned on impulsively at $t = 0$.

A series of 10 numerical experiments with parameter values listed in Table 1 were performed using the Regional Oceanic Modeling System (ROMS; Shchepetkin and McWilliams 2004). The model was run in a two-dimensional configuration (with the solutions being invariant in the zonal direction) and solved for the perturbation to the frontal-zone flow: $u'(y, z, t) \equiv u - U$ and $b'(y, z, t) \equiv b - B$, as well as for the secondary circulation in the $y - z$ plane (v, w). Lateral boundary conditions at $y = 0, L$ were periodic. Stress boundary conditions were applied at the upper and lower boundaries for the zonal and meridional velocities. All surface stresses were set to zero except for the zonal stress at $z = 0$, which was equal to the wind stress τ_o. Zero-flux boundary conditions were applied to the buoyancy at the upper and lower boundaries. The domain width and depth was $L = 12\,000$ m and $D = 250$ m, respectively. So as to adequately resolve frontal features and the Ekman layer, horizontal and vertical grid spacings of $\Delta y = 120$ m and $\Delta z = 5$ m were used. Each numerical experiment was run for 10 inertial periods.

A discussion of the subgrid-scale parameterizations

TABLE 1. Experimental parameters for numerical simulations.

Expt	S^2 (s^{-2})	f (s^{-1})	τ_o (N m^{-2})	$fS^2(\tau_o/\rho_o\delta_e)$ (m s^{-5})
A	6.3×10^{-7}	1.4×10^{-4}	0.1	3.1×10^{-16}
B	6.3×10^{-7}	1.0×10^{-4}	0.1	1.6×10^{-16}
C	6.3×10^{-7}	1.4×10^{-4}	0.5	6.8×10^{-16}
D	3.15×10^{-7}	1.4×10^{-4}	0.1	1.5×10^{-16}
E	9.5×10^{-7}	1.4×10^{-4}	0.15	5.6×10^{-16}
F	8.5×10^{-7}	1.4×10^{-4}	0.135	4.8×10^{-16}
G	9.5×10^{-7}	1.4×10^{-4}	0.1	4.6×10^{-16}
H	9.5×10^{-7}	1.4×10^{-4}	0.2	6.5×10^{-16}
I	3.15×10^{-7}	1.0×10^{-4}	0.1	0.8×10^{-16}

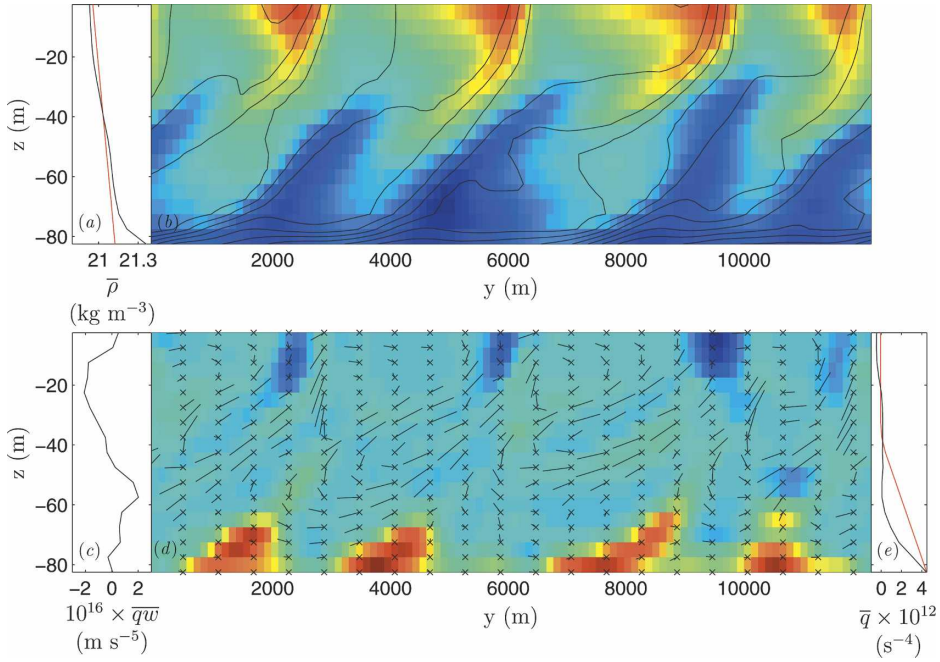

FIG. 2. Solutions from expt A at $t = 8.6$ inertial periods. (a) The meridionally averaged density (black) in comparison with a density field with a constant stratification of S^4/f^2 (red), (b) zonal velocity (shades) and density (contours) fields, (c) the meridionally averaged advective PV flux, (d) PV (shades) and secondary circulation (vectors), and (e) the meridionally averaged PV at $t = 0$ (red) and $t = 8.6$ (black) inertial periods. In both (b) and (d), warm (cool) shades indicate higher (lower) values.

used in the model is necessary, as the frictional forces and diabatic process that result from these parameterizations will play a role in the PV dynamics through the nonadvective PV flux. Diabatic processes and the zonal frictional force are parameterized in the model as

$$\mathcal{D} = \frac{\partial}{\partial z}\left(\kappa \frac{\partial b}{\partial z}\right) - \frac{\partial F^B_{\rm nl}}{\partial z} + \kappa_h \frac{\partial^4 b}{\partial y^4} \quad \text{and} \tag{12}$$

$$F^x = \frac{\partial}{\partial z}\left(\nu \frac{\partial u}{\partial z}\right) + \kappa_h \frac{\partial^4 u}{\partial y^4}, \tag{13}$$

where the eddy diffusivity of buoyancy κ (momentum ν) and nonlocal buoyancy flux $F^B_{\rm nl}$ are determined using the KPP of Large et al. (1994). As described in the appendix, the KPP scheme used in this study is modified to account for Ekman-driven convection, a process critical to the dynamics of fronts driven by downfront winds (Thomas and Lee 2005). For completeness, the biharmonic horizontal diffusion of buoyancy and momentum, with $\kappa_h = 1.7 \times 10^5$ m^4 s^{-1}, (included in the model for numerical stability) is also accounted for in (12) and (13).

b. Model solutions

A solution representative of the numerical experiments is shown in Fig. 2. As illustrated in the meridional section of the density and zonal velocity (Fig. 2b), forcing of the frontal zone by downfront winds leads to the formation of multiple fronts with sharp, frontal jets. The location of the fronts is marked by a frontal interface of enhanced lateral and vertical buoyancy gradients. The fronts form within several inertial periods as a result of frontogenetic secondary circulations characterized by upwelling along the frontal interface and downwelling of the Ekman flow (i.e., southward flow in the upper 20 m between the fronts) down the dense side of the front (Fig. 2d). Important characteristics of the solution not immediately evident in the figure are that 1) vertical vorticity at the northern sides of frontal jets is positive and exceeds f by several times and that 2) mixing of buoyancy associated with the parameterization of Ekman-driven convection is enhanced at the front. These solutions are consistent with the analytical and numerical results of Thomas and Lee (2005) that showed how Ekman pumping/suction resulting from the cross-front contrast in vertical vorticity of the frontal jet and mixing of buoyancy by Ekman-driven convection localized to the front drive frontogenetic secondary circulations. The numerical simulations of Thomas and Lee (2005) were nonhydrostatic and thus were able to explicitly resolve Ekman-driven convection. The agreement between those nonhydrostatic

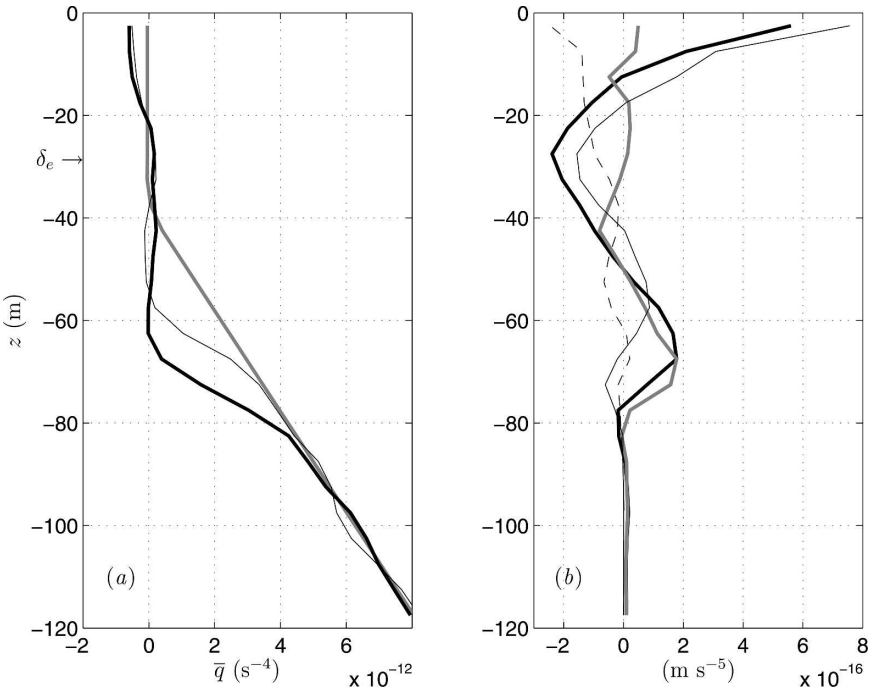

FIG. 3. (a) Meridionally averaged PV at $t = 0$ (gray), 5 (thin black), and 10 (thick black) inertial periods for expt A. (b) The meridionally averaged vertical component of the PV flux (thick black) for expt A and its constituents: the advective PV flux (gray), the frictional nonadvective flux (thin black), and the nonadvective flux associated with diabatic processes (dashed). All PV fluxes have also been averaged in time over $t = 8$–10 inertial periods.

simulations and the hydrostatic simulations presented here indicates that Ekman-driven convection and its consequences for frontal dynamics can be reproduced in a hydrostatic model using the modified version of KPP detailed in the appendix.

As evident in Fig. 2d, the secondary circulation is most intense above the strongly stratified pycnocline, yet exists in a region where the stratification of the meridionally averaged density $\overline{\rho} = -\rho_o/g\overline{b}$, where $(\overline{\ }) = (1/L)\int_0^L dy$, is nonzero (Fig. 2a). The region that the overturning motions occupy is therefore not characterized by a homogeneous density layer as with typical mixed layers, but is characterized by a "zero-PV layer" with a nearly zero meridionally averaged PV (Fig. 2e). Although it may seem somewhat paradoxical that the fluid has zero PV, yet nonzero stratification, it must be realized that for a strongly baroclinic current such as that associated with a front, the horizontal vorticity (i.e., vertical shear) and horizontal buoyancy gradients significantly contribute to the PV (1) so that the combined conditions of $q = 0$ and $\partial b/\partial z > 0$ can be met if $f\omega_a \cdot \nabla_h b < 0$, a condition that is always satisfied for a geostrophically balanced current. The zero-PV condition can be used to estimate the strength of stratification to be expected in a horizontally invariant baroclinic, geostrophic current, yielding a value $N_{\rm bc}^2 = |\overline{\nabla_h b}|^2/f^2$, where $\overline{\nabla_h b}$ is the spatially uniform horizontal buoyancy gradient of the flow (Tandon and Garrett 1994). For the idealized frontal-zone experiments, $\overline{\nabla_h b} \approx S^2$, so that $N_{\rm bc}^2 \approx S^4/f^2$. In Fig. 2a this estimate for the stratification in the zero-PV layer is tested against the numerical solution. The slope of the meridionally averaged density in the figure is well approximated by $-(\rho_o/g)S^4/f^2$.

The zero-PV layer deepens with time as high PV is eroded from the pycnocline (Fig. 3a). This erosion of PV indicates a net reduction of the total PV in the domain, a result to be expected given the arguments presented in section 2b that frictional forces by downfront winds drive a net PV flux out of the surface of the ocean and hence reduce the volume-averaged PV. Potential vorticity destruction occurs at the base of the zero-PV layer and not within the Ekman layer where frictional forces are expected to be largest; therefore, it is not obvious that friction is directly responsible for the fluxing of PV out of the pycnocline and the deepening of the layer. To determine exactly what mechanism is responsible for the PV flux out of the pycnocline, the meridionally averaged vertical component of the advective and nonadvective constituents of the PV flux were calculated (Fig. 3b). The figure illustrates that the total PV flux is upward at the base of the zero-PV layer and decays rapidly with depth, yielding a divergent flux that

therefore decreases the PV. At this depth, the PV flux is dominated by the advective PV flux, indicating that it is the secondary circulation and not friction, nor diabatic processes, that is responsible for the deepening of the zero-PV layer. The way in which the secondary circulation reduces the PV of the pycnocline is illustrated in Fig. 2d. Near the base of the zero-PV layer, upward motions advect high PV from the pycnocline, while downward motions draw low-PV waters from the surface into the pycnocline. This leads to a positive correlation between the PV and the vertical velocity, yielding an upward advective PV flux $\overline{qw} > 0$ (Fig. 2c) that extracts PV from the pycnocline and deepens the zero-PV layer. Although the frictional nonadvective PV flux plays only a minor role at the base of the zero-PV layer, in the Ekman layer it is critical. Near the surface, the frictional PV flux is large and positive, while at the base of the Ekman layer, it is negative. This vertical structure of the nonadvective, frictional PV flux leads to a PV flux divergence that maintains the low PV values in the Ekman layer. This frictionally induced source of low PV is necessary to sustain the deepening of the zero-PV layer since the secondary circulation acts only to exchange PV vertically and therefore cannot decrease the volume-averaged PV of the frontal zone. For the experiments presented here, diabatic processes do not contribute greatly to the total PV flux, a consequence of the lack of forcing by atmospheric buoyancy fluxes.

To quantitatively assess the role of the PV flux in reducing the PV in the pycnocline a PV budget was calculated. Terms in the PV budget were obtained through integrating (2) in time and space, which yields

$$\int_{z_b}^{z_t} (\overline{q}|_t - \overline{q}|_{t=0})\, dz = -\int_0^t (\overline{J}_z|_{z=z_t} - \overline{J}_z|_{z=z_b})\, dt', \tag{14}$$

where the term on the left-hand side of the equation will be referred to as the "PV deficit" and the term on the right-hand side will be called the "PV flux difference." The limits of integration for the vertical integral are constant in time and are chosen so that z_t approximately corresponds to the base of the zero-PV layer and the maximum in the advective PV flux, and z_b is at a depth at which the PV flux is weak. The time dependence of terms in the PV budget for experiment A is depicted in Fig. 4. This figure shows that, after a few inertial periods, at a stage when the flow of the secondary circulations has fully matured, the PV deficit decreases with time following the trend of the PV flux difference. Also plotted in the figure is the PV flux difference associated with the advective PV flux. The decreasing trend of the total PV flux difference is caused by the advective PV flux, yet the frictional nonadvective flux, which is negative at the base of the zero-PV layer (Fig. 3b), weakens its effect, causing the PV deficit to decrease more slowly.

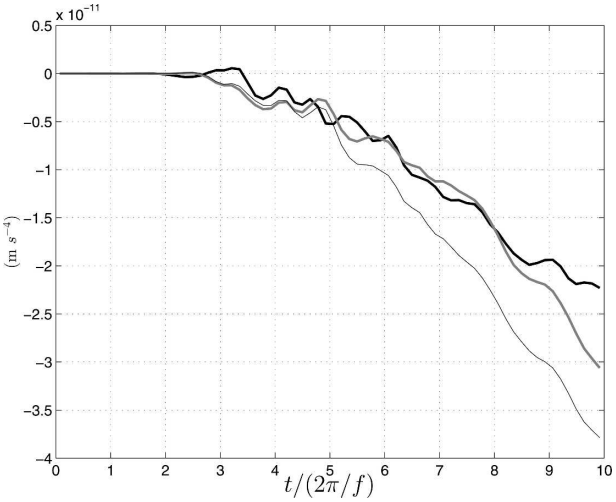

FIG. 4. Terms in the PV budget (14) in the pycnocline (z_t = −67.5 m and z_b = −107.5 m) for expt A: the PV deficit (thick black), the total PV flux difference (gray), and the advective PV flux difference (thin black).

c. Scaling of advective potential vorticity flux

In the previous section it has been discussed, using the solution from experiment A, that the extraction of PV from the pycnocline by the advective PV flux is responsible for the deepening of the zero-PV layer. In this section, the solutions from all 10 experiments (Table 1) will be used to determine how this result depends on the relevant parameters of the flow, namely, the strength of the wind stress τ_o, lateral buoyancy gradient of the frontal zone S^2, and the Coriolis parameter f. The key parameter for PV destruction by winds is the scaling of the frictional nonadvective flux (10). This is illustrated in Fig. 5, which shows that, for all the experiments, the advective PV flux at the base of the zero-PV layer increases linearly with $fS^2\tau_o/(\rho_o\delta_e)$, being smaller than this scaling by about 80%. Similarly, the magnitude of the rate of change of the PV deficit increases with $fS^2\tau_o/(\rho_o\delta_e)$, yet is smaller than the advective flux owing to the influence of the negative nonadvective frictional PV flux at the base of the zero-PV layer. The advective PV flux scales linearly with the strength of the frontal zone S^2. It should be noted, however, that this is not the case for the other parameters τ_o and f, owing to the dependence of (10) on the Ekman layer depth $\delta_e = 0.4\sqrt{\tau_o/\rho_o}/f$.

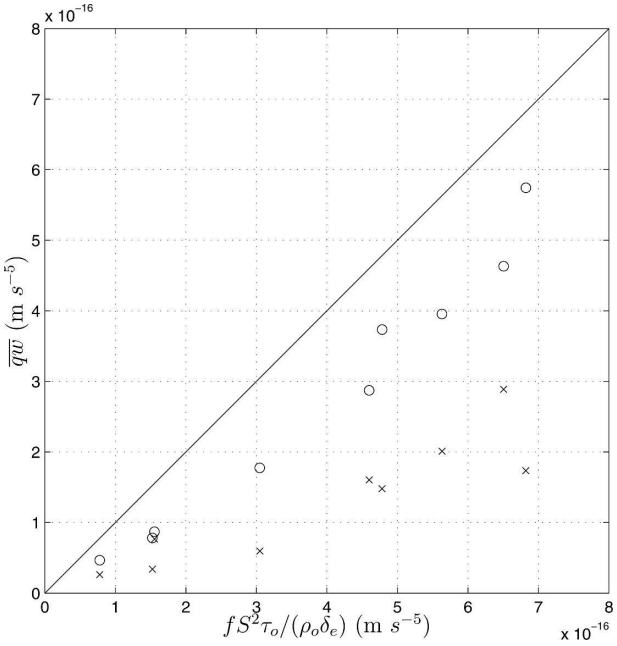

FIG. 5. Comparison of the advective PV flux $\overline{qw}$ (circles) and absolute value of the rate of change of the PV deficit (times signs) with the scaling parameter for the frictional nonadvective PV flux (10). The advective PV flux is evaluated at its maximum near the base of the zero-PV layer. Both $\overline{qw}$ and the rate of change of the PV deficit have been averaged in time over t = 8–10 inertial periods. A line with slope 1 is also plotted for reference.

4. Discussion

Many ocean fronts such as those associated with the Gulf Stream and Kuroshio, coastal upwelling systems, and the Antarctic Circumpolar Current are forced by winds that blow in the direction of the frontal jet. Forcing a front by "downfront" winds drives a nonadvective frictional PV flux that is upward at the sea surface. This PV flux extracts PV from the fluid and leads to the formation of an oceanic boundary layer with nearly zero PV and nonzero stratification. The formation of a region with zero PV and nonzero stratification has also been observed in numerical simulations of baroclinic flows forced by atmospheric buoyancy loss (e.g., Haine and Marshall 1998; Legg et al. 1998; and Straneo et al. 2002b). In such simulations, in contrast to the experiments presented here, the PV flux at the surface is provided by diabatic processes and not by frictional forces. Despite their different forcing mechanisms, both simulations exhibit a similar end result of the formation of a "zero-PV layer." This similarity indicates that the surface PV flux rather than the atmospheric buoyancy flux or wind stress is a more useful metric for describing PV destruction.

The PV-reducing effect of the frictional PV flux directly affects the Ekman layer but is transmitted through the zero-PV layer via secondary circulations that exchange low PV from the Ekman layer with high PV from the pycnocline. Averaged over the frontal zone, this PV exchange yields an upward advective PV flux that peaks at the base of the zero-PV layer and extracts PV out of the pycnocline, deepening the boundary layer. The strength of the advective PV flux and the PV deficit in the pycnocline scales with $fS^2\tau_o/(\rho_o\delta_e)$, a quantity that depends on parameters that do not vary over length scales smaller than the frontal zone. Therefore, it should be possible to parameterize PV destruction by winds in coarse-grid numerical models that cannot resolve the order-kilometer-width, frontogenetic secondary circulations but can resolve the frontal zone. A possible parameterization might involve an algorithm that 1) sets the PV in the boundary layer to zero, a method that is similar to that described in Straneo et al. (2002b) for a baroclinic flow forced by cooling, and is distinct from methods that set the stratification equal to zero as is done in standard mixed layer models; 2) modifies the PV in the pycnocline by applying a divergent PV flux that scales with $f\,S^2\tau_o/(\rho_o\delta_e)$ and has a prescribed vertical shape function; and 3) adjusts the depth of the zero-PV layer, depending on how much PV has been eroded from the pycnocline.

The impact that the parameterization described above would have on the dynamics of a coarse-grid model would depend on the grid size Δy of the model. More specifically, if the grid size of the model were so large that the maximum attainable WDBF (which is a function of S^2 and therefore decreases with increasing Δy) were much weaker than a typical atmospheric buoyancy flux forcing the model then, by (11), PV destruction by winds would not have a significant effect on the model dynamics. The maximum WDBF that can be attained in a coarse-grid model for a frontal zone with $f = 1 \times 10^{-4}$ s^{-1}, a density contrast of $\Delta\rho = 1$ kg m^{-3} (a value typical of that found in the Gulf Stream and Kuroshio systems; Fedorov 1983) and forced by a moderate downfront wind stress of $\tau_o = 0.1$ N m^{-2} is calculated in Table 2 for a range of grid sizes. In the

TABLE 2. Maximum wind-driven buoyancy flux, written as an effective heat flux (15), that can be attained in a model with a grid size Δy.

Δy (km)	$\mathcal{H}_{\text{wind}}^{\max}$ (W m^{-2})
1	20 000
10	2000
100	200
400	50

table, the maximum WDBF is written in terms of an effective heat flux; that is,

$$\mathcal{H}^{\max}_{\text{wind}} = \frac{C_w \tau_o}{\alpha \rho_o f}\left(\frac{\Delta\rho}{\Delta y}\right), \tag{15}$$

where C_w is the specific heat of water and α is the thermal expansion coefficient, in order to present the flux in more familiar units. Even for a grid size of 400 km, the WDBF is significant, suggesting that parameterizing PV destruction by winds is important for coarse grid models. However, by not adequately resolving the frontal zones of wind-forced fronts and making the fronts unrealistically diffuse, coarse-resolution models underestimate the strength of the PV sink associated with PV destruction by winds, a PV sink that may play a key role in the PV budget of the ocean. Owing to the dynamical importance of the PV to the general circulation, this inadequacy of coarse resolution models may lead to errors in simulating not only flow at frontal scales but also at the large scale.

The motivation for the present study was to investigate a possible mechanism by which wind forcing at ocean fronts forms mode water. Unlike the fluid in the zero-PV layer created by downfront winds, the low-PV fluid in mode water is found in the interior of the ocean between the seasonal and main pycnocline and is characterized by both vertical and lateral homogeneity (Hanawa and Talley 2000). Therefore, if the low-PV fluid formed by winds at fronts is to contribute to a volume of mode water, then it must be subducted and its vertical and horizontal density gradients must be diminished. Subduction occurs when the sum of the atmospheric and WDBF is downward (Nurser and Marshall 1991). This would happen at a front forced by downfront winds if the winds reversed or if the atmospheric buoyancy flux into the ocean exceeded the destabilizing WDBF. Mechanically driven subduction forced by Ekman pumping associated with wind stress curl or by ageostrophic flow set up by the meandering and/or eddying of the front itself (Spall 1995) may also be mechanisms by which the low PV at the front is drawn into the interior of the ocean. It is more likely that the latter mechanism is more effective since it drives stronger vertical velocities, with magnitudes $O(10\ \text{m day}^{-1})$ versus the $O(0.1\ \text{m day}^{-1})$ typical of the Ekman pumping (Spall 1995; Marshall et al. 1993), and because these vertical motions are localized to the front where the low PV is concentrated.

Once the low-PV fluid is subducted, although its PV is conserved, its buoyancy gradient and absolute vorticity are not, if a flow with a deformation field is present. The implication is that such a deformation field could convert the low-PV water of the zero-PV layer, with its nonzero horizontal and vertical density gradients, to a low-PV water of the mode water type with weak stratification and laterally homogeneous properties. Such dynamics cannot fully be captured in the two-dimensional numerical experiments of section 3; therefore, three-dimensional numerical simulations that either parameterize or explicitly resolve the wind-driven frontogenetic secondary circulations should be performed. A preferable configuration for the experiments would be a front associated with a separated western boundary current forced by seasonally varying winds and buoyancy fluxes. In performing such experiments, the low-PV water, its properties, and its volume could be traced through its formation and subduction phases, with the goal of assessing how viable PV destruction by downfront winds is as a contributor to mode water production.

Acknowledgments. I thank Bob Hallberg and Lu-Anne Thompson for their helpful comments and suggestions. This work was supported by the NSF Grant OCE-03-51191.

APPENDIX

Parameterization of Ekman-Driven Convection

In the *K* profile parameterization, when the ocean is forced by a destabilizing atmospheric buoyancy flux $F^B_{\text{atm}} > 0$, eddy diffusivities of tracer fields and momentum are enhanced in the the surface layer and a nonlocal buoyancy flux F^B_{nl} is applied to simulate mixing by convection. A thorough discussion of how this is implemented is given in Large et al. (1994). The key features of this implementation that are relevant to the parameterization for Ekman-driven convection are that the strength of the eddy diffusivity is set by the depth of the mixed layer H and the convective velocity scale $w^* = (F^B_{\text{atm}} H)^{1/3}$ and that convective mixing of buoyancy is parameterized using a nonlocal buoyancy flux that follows the form $F^B_{\text{nl}} = F^B_{\text{atm}} G(z/H)$, where $G(z/H)$ is a vertical shape function. As was shown by Thomas and Lee (2005) using nonhydrostatic numerical experiments of a frontal zone forced by downfront winds, close to fronts, the nonlocal convective buoyancy flux associated with Ekman-driven convection scales with the WDBF. Its vertical structure (equal to zero at the surface, maximum near the base of the Ekman layer, decaying with depth, turning negative near the base of the mixed layer, and equal to zero at the base of the mixed layer) is well captured by the vertical shape functions used in the KPP. It therefore follows that a simple

parameterization for Ekman-driven convection that is consistent with the results of the nonhydrostatic simulations of Thomas and Lee (2005) would involve modifying the KPP mixing scheme to have the nonlocal buoyancy flux be scaled by both the atmospheric buoyancy flux and the WDBF:

$$F^B_{\rm nl} = (F^B_{\rm atm} + F^B_{\rm wind})G\left(\frac{z}{H}\right), \tag{A1}$$

and to have the convective velocity scale include a contribution from the WDBF:

$$w^* = [(F^B_{\rm atm} + F^B_{\rm wind})H]^{1/3}. \tag{A2}$$

This parameterization was used in the hydrostatic simulations of section 3, where the WDBF in (A1) and (A2) was calculated by vertically integrating the horizontal advection of buoyancy term, $-\mathbf{u}\cdot\nabla_h b$, through the Ekman layer. More specifically, if this integral is negative (which occurs when the Ekman flow advects dense water over light and destabilizes the water column), the WDBF is equal to the absolute value of the integral and zero otherwise:

$$F^B_{\rm wind} \equiv \frac{1}{2}\left(\left|-\int_{-\delta_e}^{0}\mathbf{u}\cdot\nabla_h b\,dz\right| + \int_{-\delta_e}^{0}\mathbf{u}\cdot\nabla_h b\,dz\right). \tag{A3}$$

By setting $F^B_{\rm wind}$ equal to zero when the integral is positive, the KPP mixing scheme does not interfere with the numerical model's algorithm for advecting buoyancy and allows flow in the Ekman layer to stratify the water column.

REFERENCES

Chereskin, T. K., and D. Roemmich, 1991: A comparison of measured and wind-derived Ekman transport at 11°N in the Atlantic Ocean. *J. Phys. Oceanogr.,* **21,** 869–878.

Fedorov, K. N., 1983: *The Physical Nature and Structure of Oceanic Fronts.* Springer-Verlag, 333 pp.

Haine, T. W. N., and J. Marshall, 1998: Gravitational, symmetric, and baroclinic instability of the ocean mixed layer. *J. Phys. Oceanogr.,* **28,** 634–658.

Hanawa, K., and L. D. Talley, 2000: Mode waters. *Ocean Circulation and Climate,* G. Siedler and J. Church, Eds., Academic Press, 373–386.

Haynes, P., and M. McIntyre, 1987: On the evolution of vorticity and potential vorticity in the presence of diabatic heating and frictional or other forces. *J. Atmos. Sci.,* **44,** 828–841.

Hoskins, B. J., 1974: The role of potential vorticity in symmetric stability and instability. *Quart. J. Roy. Meteor. Soc.,* **100,** 480–482.

Large, W. G., J. C. McWilliams, and S. C. Doney, 1994: Oceanic vertical mixing: A review and a model with a nonlocal boundary layer parameterization. *Rev. Geophys.,* **32,** 363–403.

Lee, C. M., and C. C. Eriksen, 1996: The subinertial momentum balance of the North Atlantic subtropical convergence zone. *J. Phys. Oceanogr.,* **26,** 1690–1704.

Legg, S., J. McWilliams, and J. Gao, 1998: Localization of deep convection by a mesoscale eddy. *J. Phys. Oceanogr.,* **28,** 944–970.

Marshall, J. C., and A. J. G. Nurser, 1992: Fluid dynamics of oceanic thermocline ventilation. *J. Phys. Oceanogr.,* **22,** 583–595.

——, ——, and R. G. Williams, 1993: Inferring the subduction rate and period over the North Atlantic. *J. Phys. Oceanogr.,* **23,** 1315–1329.

Nurser, A. J. G., and J. C. Marshall, 1991: On the relationship between subduction rates and diabatic forcing of the mixed layer. *J. Phys. Oceanogr.,* **21,** 1793–1802.

Rhines, P. B., 1986: Vorticity dynamics of the oceanic general circulation. *Annu. Rev. Fluid Mech.,* **18,** 433–497.

Rintoul, S. R., and M. H. England, 2002: Ekman transport dominates local air–sea fluxes in driving variability of Subantarctic Mode Water. *J. Phys. Oceanogr.,* **32,** 1308–1321.

Shchepetkin, A. F., and J. C. McWilliams, 2004: The Regional Ocean Modeling System (ROMS): A split-explicit, free-surface, topography-following coordinate oceanic model. *Ocean Modell.*, **9,** 347–404.

Spall, M. A., 1995: Frontogenesis, subduction, and cross-front exchange at upper ocean fronts. *J. Geophys. Res.,* **100,** 2543–2557.

Straneo, F., M. Kawase, and R. S. Pickart, 2002a: Effects of wind on convection in strongly and weakly baroclinic flows with application to the Labrador Sea. *J. Phys. Oceanogr.,* **32,** 2603–2618.

——, ——, and S. Riser, 2002b: Idealized models of slantwise convection in a baroclinic flow. *J. Phys. Oceanogr.,* **32,** 558–572.

Tandon, A., and C. Garrett, 1994: Mixed layer restratification due to a horizontal density gradient. *J. Phys. Oceanogr.,* **24,** 1419–1424.

Thomas, L. N., and C. M. Lee, 2005: Intensification of ocean fronts by down-front winds. *J. Phys. Oceanogr.,* **35,** 1086–1102.

Wijffels, S., E. Firing, and H. Bryden, 1994: Direct observation of the Ekman balance at 10°N in the Pacific. *J. Phys. Oceanogr.,* **24,** 1666–1679.

Wimbush, M., and W. Munk, 1970: The benthic boundary layer. *The Sea*, M. N. Hill, Ed., New Concepts of Sea Floor Evolution, Part II: Regional Observations and Concepts, Vol. 4, Wiley and Sons, 731–758.

Worthington, L. V., 1977: Intensification of the Gulf Stream after the winter of 1976–1977. *Nature,* **270,** 415–417.